

International Journal of Modern Physics: Conference Series
 © World Scientific Publishing Company

A comparative study of non-Gaussianity in ILC-7yr CMB map

WILMAR A. CARDONA

*Centro Brasileiro de Pesquisas Físicas, Rua Dr. Xavier Sigaud 150
 22290-180 Rio de Janeiro – RJ, Brazil*

ARMANDO BERNUI

*Instituto de Ciências Exatas, Universidade Federal de Itajubá
 37500-903 Itajubá – MG, Brazil*

MARCELO J. REBOUÇAS

*Centro Brasileiro de Pesquisas Físicas, Rua Dr. Xavier Sigaud 150
 22290-180 Rio de Janeiro – RJ, Brazil*

Received Day Month Year

Revised Day Month Year

A detection or non detection of primordial non-Gaussianity (NG) by using the cosmic microwave background radiation (CMB) is a possible way to break the degeneracy of early universe models. Since a single statistical estimator hardly can be sensitive to all possible forms of NG which may be present in the data, it is important to use different statistical estimators to study NG in CMB. Recently, two new large-angle NG indicators based on skewness and kurtosis of spherical caps or spherical cells of CMB sky have been proposed and used in both CMB data and simulated maps. Here, we make a comparative study of these two different procedures by examining the NG in the WMAP seven years ILC map. We show that the spherical cells procedure detects a higher level of NG than that obtained by the method with overlapping spherical caps.

Keywords: Gaussianity; cosmic microwave background, inflation, physics of the early universe.

PACS numbers: 98.80.Es, 98.70.Vc, 98.80.-k

1. Introduction

Recent CMB cosmological observations are compatible with a nearly scale invariant power spectrum. However, there are many models of early universe that fit CMB data.¹ This gives rise to the need of further ways of testing the models of primordial universe. A possible way to break the degeneracy in the models of the early universe is by studying deviation of Gaussianity of CMB data.^{2–3} Thus, for example, in a single-field model of inflation, the amplitude $f_{\text{NL}}^{\text{local}}$ of the three-point correlation function counterpart in Fourier space — the so-called bispectrum — can be calculated in terms of the slow-roll parameters and is very tiny ($f_{\text{NL}}^{\text{local}} \lesssim 10^{-6}$).⁴ Hence,

2 *Wilmar A. Cardona, Armando Bernui, Marcelo J. Rebouças*

any convincing detection of $f_{\text{NL}}^{\text{local}} \gg 1$ indicate a clear departure from the slow-roll inflationary paradigm. On the other hand, if a no significant $f_{\text{NL}}^{\text{local}}$ is found from CMB observation, the standard slow-roll scenario would clearly be favored.

In the study of NG in the CMB data one ought to take into account that there are contributions which do not have a primordial origin. Some non-primordial contributions come from unsubtracted diffuse foreground emission,^{5–6} unresolved point sources,⁷ possible systematic errors,⁸ and secondary anisotropies such as gravitational weak lensing and the Sunyaev–Zeldovich effect.^{2–9} Deviation from Gaussianity may also have a cosmic topology origin (see, e.g., the review articles Refs. 10). Different statistical tools can provide information from distinct contributions to the NG in CMB data (see, for example, Ref. 15 and references therein). Furthermore, since a single statistical estimator hardly can be sensitive to all possible contributions to NG that may exist, it is useful to use different statistical tools to test CMB data for deviations from a Gaussian statistics in order to quantify the amount of any non-Gaussian signals in the data, and extract information on their possible origins.

Recently, two new large-angle NG indicators based on skewness and kurtosis of spherical caps or spherical cells of CMB sky have been proposed and used in both CMB data and simulated maps.^{11–13} In this work, we make a comparative study of these two different procedures by examining the NG in the WMAP ILC–7 map. We show that the spherical cells procedure detects a higher level of NG than that obtained by the method with overlapping spherical caps.

2. Statistical estimators and Non-Gaussianity in ILC–7 yr map

A simple way for describing deviation from a Gaussian distribution in CMB temperature fluctuations is by calculating skewness

$$S = \frac{\mu_3}{\sigma^3}, \quad (1)$$

and kurtosis

$$K = \frac{\mu_4}{\sigma^4} - 3, \quad (2)$$

where σ , μ_3 and μ_4 are, respectively, the second, third and fourth central moments of the distribution. Based upon the fact that S and K vanish for a Gaussian distribution, two statistical indicators to measure large-angle NG in CMB were introduced in Ref. 11. The constructive process can be formalized as follows. Let $\Omega_j \equiv \Omega(\theta_j, \phi_j) \in S^2$ be set of points in a spherical region. For $j = 1, \dots, N$, we define scalar functions $S : \Omega_j \rightarrow \mathbb{R}$ and $K : \Omega_j \rightarrow \mathbb{R}$, that assign to the j^{th} spherical region two real numbers given by

$$S_j \equiv \frac{1}{N_p \sigma_j^3} \sum_{i=1}^{N_p} (T_i - \overline{T_j})^3 \quad (3)$$

and

$$K_j \equiv \frac{1}{N_p \sigma_j^4} \sum_{i=1}^{N_p} (T_i - \overline{T_j})^4 - 3, \quad (4)$$

where N_p is the number of pixels in the j^{th} spherical region, T_i is the temperature at the i^{th} pixel, $\overline{T_j}$ and σ_j are, respectively, the CMB mean temperature and the variance

$$\sigma_j^2 = \frac{1}{N_p - 1} \sum_{i=1}^{N_p} (T_i - \overline{T_j})^2. \quad (5)$$

in the j^{th} region.

In the next two section we shall use this constructive process to formalize two different procedures which allow to build skewness and kurtosis $S(\theta, \phi)$ and $K(\theta, \phi)$ functions from a given input CMB map. The major difference of the two methods is the way one chooses the spherical region to define these functions.

2.1. Spherical caps method

In this method one chooses for the spherical region, Ω_j , overlapping spherical caps in order to define $S(\theta, \phi)$ and $K(\theta, \phi)$ functions on the sphere. The procedure to build these functions is as follows.

- (i) For a given CMB map we take a discrete set of points $j = 1, \dots, N_c$ homogeneously distributed on the celestial sphere S^2 as the center of spherical caps (spherical region Ω_j) with aperture γ .
- (ii) Then, one calculates skewness (S_j) and kurtosis (K_j) for each spherical cap j defined, respectively, by Eqs. (3)–(4).
- (iii) Patching together the S_j and K_j values for each spherical cap we obtain two discrete functions $S(\theta, \phi)$ and $K(\theta, \phi)$ defined on the celestial sphere S^2 . These functions can be used to measure NG as a function of the angular coordinates (θ, ϕ) . The Mollweid projection of skewness and kurtosis functions $S = S(\theta, \phi)$ and $K = K(\theta, \phi)$ are skewness and kurtosis maps which we shall refer hereafter as S map and K map, respectively.

Fig. 1 shows S and K maps calculated from the WMAP ILC-7 yr map by using the spherical cap procedure.^a

^aIn this work all the CMB maps we use to generate S and K maps have HEALPix parameter $N_{\text{side}} = 256$ as defined in Ref. 16. This means that each spherical cap has $N_p = 393\,216$ pixels. On the other hand, all S and K maps generated with the spherical caps method have $N_c = 3\,072$ and $\gamma = 90^\circ$.

4 Wilmar A. Cardona, Armando Bernui, Marcelo J. Rebouças

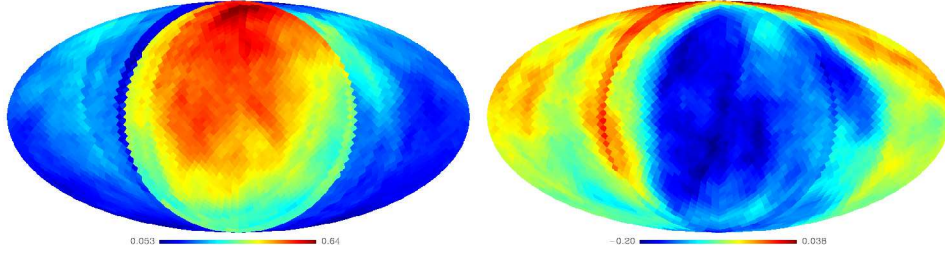


Fig. 1. Kurtosis indicator map (left panel) and skewness indicator map (right panel) generated from the WMAP seven years ILC map by using the spherical caps method with $N_c = 3072$.

2.2. Spherical cells method

Differently from the spherical caps method of the previous section, in the spherical cells method one considers non-overlapping region of the CMB sphere, generated by the HEALPix partition of the sphere, for defining $S(\theta, \phi)$ and $K(\theta, \phi)$ functions. The procedure to build the indicators is as follows.

- (i) For a given CMB map we divide the CMB sphere into 12 equal area primary spherical cells by using the HEALPix partition of the sphere.
- (ii) We divide each one of the 12 primary cells, in which the HEALPix partition divides initially the sphere, in N'_{side} new spherical cells. Thus, we obtain $N'_p = 12 \times N'^2_{\text{side}}$ spherical cells on the whole sphere.
- (iii) To define $S(\theta, \phi)$ and $K(\theta, \phi)$ functions on the sphere, in each one of the N'_p spherical cells we calculate skewness and kurtosis by using Eqs. (3)–(4) with N_p and σ_j being, respectively, the number of pixels and the variance in each cell.
- (iv) Finally, patching together S_j and K_j ($j = 1, 2, \dots, N'_p$) we define discrete functions of skewness $S(\theta, \phi)$ and kurtosis $K(\theta, \phi)$ on the celestial sphere S^2 . As in the spherical caps method, the Mollweid projection of these functions constitutes S and K maps, respectively.

Fig. 2 shows S and K maps calculated from the WMAP ILC-7 yr by taking 48 spherical cells each one with $N_p = 16\,384$ temperature fluctuation pixels.

2.3. Comparative analysis

In this section we shall make a comparative study of these two different procedure to construct the S and K indicators by examining the NG in the WMAP ILC-7 yr map. To this end, we first compute angular power spectra S_ℓ and K_ℓ of S and K maps generated from both a set of 1000 Gaussian CMB simulated maps and from the WMAP seven years ILC map. Then, we use χ^2 statistics to compare the sets of mean angular power spectra $\overline{S_\ell^G}$ and $\overline{K_\ell^G}$ of S and K Gaussian simulated CMB maps, with the angular power spectra, S_ℓ^{ILC} and K_ℓ^{ILC} calculated from S and K

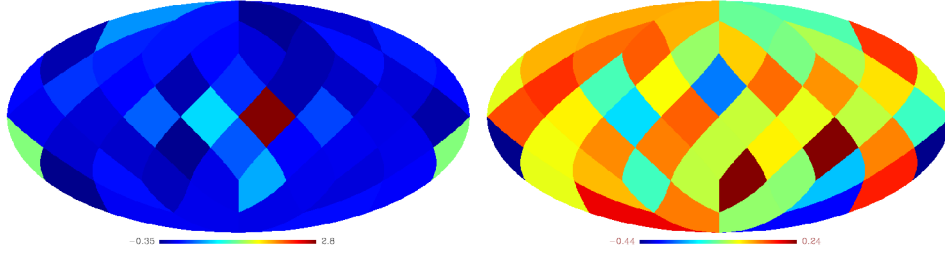


Fig. 2. Kurtosis indicator map (left panel) and skewness indicator map (right panel) generated from the WMAP seven years ILC map by using the spherical cells method with 48 spherical cells ($N'_{\text{side}} = 4$). Each colored division is a spherical cell.

maps generated from the WMAP ILC-7 yr map. The procedure is as follows.

- (i) We use 1000 Gaussian CMB simulated maps which were built by using the procedure explained in Ref. ?.^b
- (ii) We generate S and K maps both for the set of 1000 Gaussian CMB simulated maps and for the ILC-7 yr map.
- (iii) We expand the functions $S(\theta, \phi)$ and $K(\theta, \phi)$ corresponding to the S and K maps of the item (ii) in spherical harmonics as

$$\begin{aligned}
 K(\theta, \phi) &= \sum_{\ell=0}^{\infty} \sum_{m=-\ell}^{\ell} b_{\ell m} Y_{\ell m}(\theta, \phi), \\
 S(\theta, \phi) &= \sum_{\ell=0}^{\infty} \sum_{m=-\ell}^{\ell} b'_{\ell m} Y_{\ell m}(\theta, \phi),
 \end{aligned} \tag{6}$$

and find the corresponding angular power spectra given by

$$\begin{aligned}
 K_{\ell} &= \frac{1}{2\ell+1} \sum_m |b_{\ell m}|^2, \\
 S_{\ell} &= \frac{1}{2\ell+1} \sum_m |b'_{\ell m}|^2.
 \end{aligned} \tag{7}$$

- (iv) For the sets of Gaussian CMB simulated maps we also calculate the mean value $\overline{S_{\ell}}$ and $\overline{K_{\ell}}$ and their variance.
- (v) Finally, we calculate χ^2 for S and K maps given by

^bThese maps were made available to download in <http://planck.mpa-garching.mpg.de/cmb/fnl-simulations>.

6 *Wilmar A. Cardona, Armando Bernui, Marcelo J. Rebouças*

$$\chi_{S_\ell}^2 = \frac{1}{3} \sum_{\ell=1}^4 \frac{(S_\ell^{\text{ILC}} - \overline{S_\ell^{\text{G}}})^2}{\sigma_\ell^{\text{G}^2}}, \quad (8)$$

and

$$\chi_{K_\ell}^2 = \frac{1}{3} \sum_{\ell=1}^4 \frac{(K_\ell^{\text{ILC}} - \overline{K_\ell^{\text{G}}})^2}{\sigma_\ell^{\text{G}^2}}. \quad (9)$$

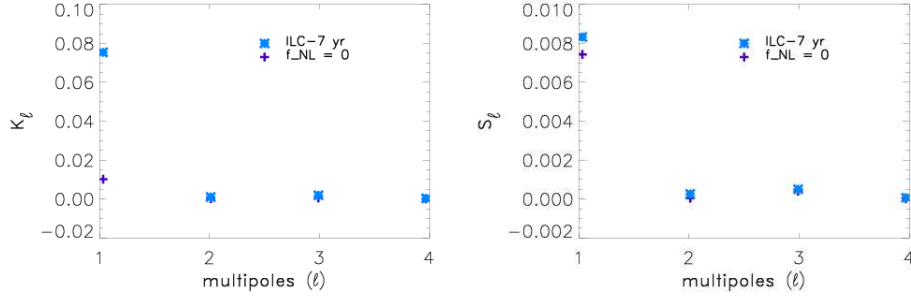


Fig. 3. Low ℓ angular power spectrum of skewness S_ℓ (right panel) and kurtosis K_ℓ (left panel) maps calculated from ILC-7 yr and Gaussian CMB simulated maps by using the spherical caps method.

Table 1. χ^2 test goodness of fit for S_ℓ^{ILC} and K_ℓ^{ILC} as compared with $\overline{S_\ell^{\text{G}}}$ and $\overline{K_\ell^{\text{G}}}$.

Method	$\chi_{S_\ell}^2$	$\chi_{K_\ell}^2$
Cells	6.27×10	6.25×10^3
Caps	4.07	2.04×10

Fig. 3 and Fig. 4 show the angular power spectra for S and K maps calculated by using the spherical caps method and the cells method, respectively. Fig.3 makes apparent the tiny difference in the power of the spectra $\overline{S_\ell^{\text{G}}}$ ($\overline{K_\ell^{\text{G}}}$) and S_ℓ^{ILC} (K_ℓ^{ILC}). On the other hand, Fig. 4 exhibits bigger differences between $\overline{S_\ell^{\text{G}}}$ ($\overline{K_\ell^{\text{G}}}$) and S_ℓ^{ILC} (K_ℓ^{ILC}) making showing qualitatively that the spherical cells method capture a greater departure for the ILC-7 yr map than that detected through the spherical method.

To obtain quantitative information regarding the sensitivity to detect deviation from Gaussianity by S and K indicators built by using both spherical caps method and spherical cells method, we perform a χ^2 test to determine the goodness of fit

A comparative study of non-Gaussianity in ILC-7yr

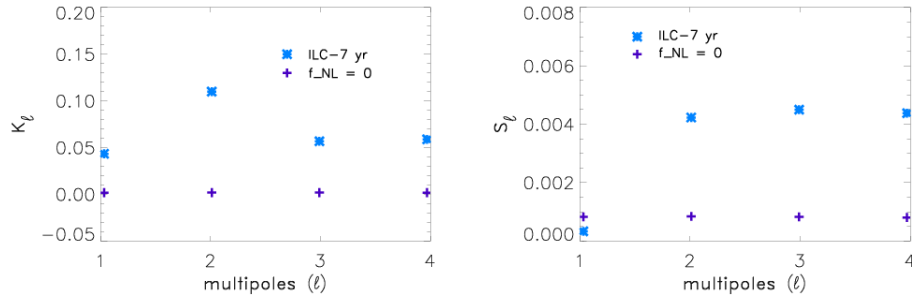


Fig. 4. Low ℓ angular power spectrum of skewness S_ℓ (right panel) and kurtosis K_ℓ (left panel) maps calculated from ILC-7 yr and Gaussian CMB simulated maps by using the spherical cells method.

for S_ℓ^{ILC} (K_ℓ^{ILC}) as compared with $\overline{S_\ell^{\text{G}}}$ ($\overline{K_\ell^{\text{G}}}$). Since a good fit occurs when $\chi^2 \approx 1$, results collected together in Table 1 make apparent that, for the ILC-7 yr map, the spherical cells method capture a greater degree of NG than that detected through the spherical method.

Acknowledgments

M.J. Rebouças acknowledges the support of FAPERJ under a CNE E-26/101.556/2010 grant. This work was also supported by Conselho Nacional de Desenvolvimento Científico e Tecnológico (CNPq) - Brasil, under grant No. 475262/2010-7. A. Bernui thanks FAPEMIG for the grant APQ-01893-10. M.J. Rebouças, Wilmar A. Cardona and A. Bernui thank CNPq for the grants under which this work was carried out. Some of the results in this paper were derived using the HEALPix package.¹⁶

References

1. B.A. Bassett, S. Tsujikawa, and D. Wands, *Rev. Mod. Phys.* **78**, 537 (2006); A. Linde, *Lect. Notes Phys.* **738**, 1 (2008).
2. E. Komatsu, *Class. Quant. Grav.* **27**, 124010 (2010).
3. N. Bartolo, E. Komatsu, S. Matarrese, and A. Riotto, *Phys. Rept.* **402**, 103 (2004).
4. V. Acquaviva, N. Bartolo, S. Matarrese, and A. Riotto, *Nucl. Phys. B* **667**, 119 (2003); J. Maldacena, *JHEP* **0305** 013 (2003); M. Liguori, F.K. Hansen, E. Komatsu, S. Matarrese, and A. Riotto, *Phys. Rev. D* **73**, 043505 (2006).
5. C.L. Bennett *et al.*, *Astrophys. J. Suppl.* **148**, 97 (2003).
6. S.M. Leach *et al.*, *Astron. Astrophys.* **491**, 597 (2008).
7. E. Komatsu *et al.*, *Astrophys. J. Suppl.* **148**, 119 (2003).
8. M. Su, A.P.S. Yadav, M. Shimon, B.G. Keating, *Phys. Rev. D* **83**, 103007 (2011).
9. M. Liguori, E. Sefusatti, J.R. Fergusson, and E.P.S. Shellard, *Adv. Astron.* **2010**, 980523 (2010).
10. G.F.R. Ellis, *Gen. Rel. Grav.* **2**, 7 (1971); M. Lachièze-Rey and J.-P. Luminet, *Phys. Rep.* **254**, 135 (1995); G.D. Starkman, *Class. Quantum Grav.* **15**, 2529 (1998); J.-P.

8 *Wilmar A. Cardona, Armando Bernui, Marcelo J. Rebouças*

- Uzan, R. Lehoucq, and J-P. Luminet, arXiv:gr-qc/0005128; J. Levin, *Phys. Rep.* **365**, 251 (2002); M.J. Rebouças and G. I. Gomero, *Braz. J. Phys.* **34**, 1358 (2004); M.J. Rebouças, arXiv:astro-ph/0504365; M.C. Bento, O. Bertolami, M.J. Rebouças, P.T. Silva, *Phys. Rev. D* **73**, 043504 (2006).
11. A. Bernui and M.J. Rebouças, *Phys. Rev. D* **79**, 063528 (2009).
 12. A. Bernui and M.J. Rebouças, *Phys. Rev. D* **81**, 063533 (2010).
 13. A. Bernui and M.J. Rebouças, *Phys. Rev. D* **85**, 023522 (2012).
 14. W.A. Cardona, A. Bernui, and M.J. Rebouças, in preparation (2013).
 15. A. Bernui, B. Mota, M.J. Rebouças, and R. Tavakol, *Astron. & Astrophys.* **464**, 479 (2007); A. Bernui, B. Mota, M.J. Rebouças, and R. Tavakol, *Int. J. Mod. Phys. D* **16**, 411 (2007). R. Saha, *Astrophys. J. Letters*, **739**, L56 (2011); C. Räth, G.E. Morfill, G. Rossmannith, A.J. Banday, and K.M. Górski, *Phys. Rev. Lett.* **102**, 131301 (2009); G. Rossmannith, C. Räth, A.J. Banday, and G. Morfill, *Mon. Not. R. Astron. Soc.* **399**, 1921 (2009); C. Räth, P. Schuecker, and A.J. Banday, *Mon. Not. R. Astron. Soc.* **380**, 466 (2007); N. Mandolesi, C. Burigana, A. Gruppuso, and P. Natoli, *J. Phys. Conf. Ser.* **335**, 012009 (2011); A. Gruppuso, F. Finelli, P. Natoli, F. Paci, P. Cabella, A. De Rosa, and N. Mandolesi, *Mon. Not. R. Astron. Soc.* **411**, 1445 (2011), S.-Y. Zhong, X. Wu, S.-Q. Liu, and X.-F. Deng, *Phys. Rev. D* **82**, 124040 (2010); S.-Y. Zhong and X. Wu, *Phys. Rev. D* **81**, 104037 (2010); A. Bernui, M.J. Rebouças, and A.F.F. Teixeira, arXiv:1005.0883 [astro-ph.CO]; A. Bernui, M.J. Rebouças, and A.F.F. Teixeira, *Int. J. Mod. Phys. Conf. Ser.* **3**, 286 (2011); V.N. Yershov, V.V. Orlov, and A.A. Raikov, arXiv:1205.5139 [astro-ph.CO].
 16. K.M. Górski, E. Hivon, A.J. Banday, B.D. Wandelt, F.K. Hansen, M. Reinecke, and M. Bartelman, *Astrophys. J.* **622**, 759 (2005).